A Model to Optimize a Microwave PBG Accelerator Based on Generic Unit Cell

Roberto Diana Laboratorio di Dispositivi Elettronici, Politecnico di Bari, Dipartimento di Elettrotecnica ed Elettronica, via E. Orabona, 4, 70125 Bari, Italy

Agostino Giorgio Laboratorio di Dispositivi Elettronici, Politecnico di Bari, Dipartimento di Elettrotecnica ed Elettronica, via E. Orabona, 4, 70125 Bari, Italy

Roberto Marani Laboratorio di Dispositivi Elettronici, Politecnico di Bari, Dipartimento di Elettrotecnica ed Elettronica, via E. Orabona, 4, 70125 Bari, Italy

Vittorio M. N. Passaro Laboratorio di Dispositivi Elettronici, Politecnico di Bari, Dipartimento di Elettrotecnica ed Elettronica, via E. Orabona, 4, 70125 Bari, Italy

Anna Gina Perri perri@poliba.it Laboratorio di Dispositivi Elettronici, Politecnico di Bari, Dipartimento di Elettrotecnica ed Elettronica, via E. Orabona, 4, 70125 Bari, Italy

In this paper a numerical method, based on the well known Floquet–Bloch theory, useful to analyze the physical properties of a PBG based accelerator, is presented. The proposed model has been developed to analyze a 2D lattice characterized by a generic inclination angle between the two primitive translation vectors, thus resulting very useful when a periodic structure without an equilateral triangular or square cell has to be investigated. The numerical method has been optimized in order to account several number of space harmonics with a low CPU time and memory consumption. Comparisons with more complex numerical methods demonstrate the accuracy of our model. Several simulations have been performed to find all the geometrical parameters including the inclination angle of the unit cell, filling factor and index contrast. The proposed method, through an optimization procedure of the photonic band structure, allows to obtain a large spectral purity, high order mode suppression and high Q–values. [DOI: 10.2971/jeos.2007.07006]

Keywords: Photonic bandgap (PBG), photonic crystals, microwave signal processing, microwave photonics

1 Introduction

Recently a significant research on microwave particle accelerator devices for medical applications has received an increasing interest due to the PBG properties to control the light flow by a periodic plane (2D) arrangement of metallic or dielectric rods placed in a dielectric medium having a different refractive index [1, 2]. These structures are particularly suitable when modal selectivity and strong field confinement are required, and very performing resonant cavities characterized by high Q–factor can be easily designed and realized. One of the most important characteristics of a PBG–based resonant cavity is the efficient suppression of the Higher–Order Modes (HOM) and wakefields. This makes such structures very attractive for their high efficiency and low cost for medical applications, particularly in the field of the heavy particle acceleration to be used in the hadrontherapy for cancer treatment.

A rigorous analysis of the physical effects occurring when a wave propagates inside a periodic structure requires a complex theoretical investigation, which has to take into account all the involved geometrical parameters without any conceptual approximation.

The Floquet–Bloch theory, applied by the Authors before to analyze 1D periodic structures on planar waveguide [3, 4] and after to study the physical properties of optical fiber Bragg gratings [5, 6], allows to perform fast investigations and the results are more accurate than those obtained from other numerical methods already compared in a previous work [3]. The numerical approach based on the Floquet–Bloch theory has next been extended to analyze two–dimensional multilayer photonic bandgap structures with a typical triangular or square lattice [7], where the physical features of the investigated devices, working at microwave or optical frequency range, can be optimized in terms of band structure. The forbidden frequency range, arising from the periodic geometry of the photonic device, can be enlarged in order to improve the spectral purity of a "defect mode" which can be forced inside the bandgap by removing a dielectric rod and, then, breaking the periodicity of the crystal. The optimization of the photonic band structure, achieved in [7] by choosing the best value of filling factor and dielectric rod permittivity, is relevant only to the high symmetrical structures characterized by an equilateral triangular or square cell.

In this paper we have improved our method [7] to characterize photonic crystals having a lattice with a generic inclination angle between the primitive translation vectors thus obtaining a high numerical stability.

To validate our model, some comparisons of the results with

Received October 31, 2006; published January 25, 2007 ISSN 1990-2573

those of other more complex methods, such as Finite Domain Time Division method (FDTD), have been performed. Next we have applied our approach to a PBG–based particle accelerator. All the relationships required to define the Brillouin region for a 2D lattice with generic unit cell are presented in section 2. Several numerical simulations and comparisons, reported in section 3, have been performed to evaluate, for the device under investigation, the best values of geometrical parameters such as the inclination angle of the unit cell and the filling factor.

2 THEORY

Figure 1 shows the investigated structure, constituted by circular section dielectric rods periodically arranged according to a two–dimensional grating. The dielectric rods, having permittivity ϵ_a and embedded in a dielectric medium with permittivity ϵ_b, are placed at the vertices of a generic primitive unit cell. The primitive translation vectors $\mathbf{a}_1$ and $\mathbf{a}_2$ are noncollinear and inclined at angle γ. The particular cases of $\gamma = \pi/2$ or $\gamma = \pi/3$ correspond to a square or hexagonal lattice, respectively.

The charged particles must be accelerated with high efficiency along a direction (x axis) perpendicular to the periodicity plane (yz plane), thus requiring the tangential components of the electric field to vanish everywhere. This field distribution, also characterized by a magnetic field vector in periodicity plane (TM mode), can be forced by enclosing the 2D array between two metallic layers, which are assumed to be lossless. The device has to be designed to produce an allowed mode inside a forbidden frequency range, i.e. a bandgap, in order to improve the spectral purity.

The grating parameters R, a, t_g are the rod radius, the lattice constant (amplitude of the primitive translation vectors) and rod height, respectively.

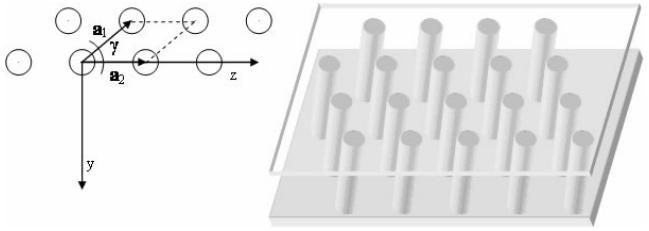

FIG. 1 Primitive unit cell with its translation vectors (a) and architecture of the microwave particle accelerator (b)

The primitive translation vectors $\mathbf{a}_1$ and $\mathbf{a}_2$ are defined by the relations:

$$\begin{aligned} \mathbf{a}_1 &= -a\sin(\gamma)\,\hat{\mathbf{y}} + a\cos(\gamma)\,\hat{\mathbf{z}} \\ \mathbf{a}_2 &= a\hat{\mathbf{z}} \end{aligned} \tag{1}$$

$\hat{\mathbf{y}}$ and $\hat{\mathbf{z}}$ are the unit vectors along the axes of the periodicity plane. From the previous assumption it follows that primitive translation vectors of the reciprocal lattice are given by [8]:

$$\begin{aligned} \mathbf{b}_1 &= -\tfrac{2\pi}{a}\tfrac{1}{\sin(\gamma)}\hat{\mathbf{y}} \\ \mathbf{b}_2 &= \tfrac{2\pi}{a}\left(\tfrac{\hat{\mathbf{y}}}{\tan(\gamma)} + \hat{\mathbf{z}}\right) \end{aligned} \tag{2}$$

In order to calculate the photonic band diagram for waves propagating in a plane perpendicular to the dielectric rods, we have to expand all the components of the electromagnetic field according the Floquet–Bloch theorem. To this purpose, the inverse permittivity function can be expressed in the periodic region (the yz plane) as a Fourier–series:

$$\epsilon^{-1}(\boldsymbol{\rho}) = \sum_{\mathbf{G}\in G} \epsilon_G^{-1}(\mathbf{G})\, e^{j\mathbf{G}\cdot\boldsymbol{\rho}} \tag{3}$$

where $\mathbf{G}$ is the generic reciprocal lattice vector. For cylindrical rods we have:

$$\epsilon_G^{-1}(\mathbf{G}) = \begin{cases} \frac{1}{\epsilon_a}f + \frac{1}{\epsilon_b}(1-f) & \mathbf{G}=\mathbf{0} \\ (\frac{1}{\epsilon_a} - \frac{1}{\epsilon_b}) f \frac{2J_1(|\mathbf{G}|R)}{|\mathbf{G}|R} & \mathbf{G}\neq\mathbf{0} \end{cases} \tag{4}$$

where the filling factor $f = a_R/a_C$ is the fraction of the area a_C of the unit cell occupied by the area a_R of the rod; in our case it results:

$$f = \pi\left(\frac{R}{a}\right)^2 \frac{1}{\sin(\gamma)} \tag{5}$$

According to the Floquet–Bloch formalism, the field components can be expressed as the superposition of an infinite number of space harmonics. Then, assuming $\Psi_\xi = E_\xi, H_\xi$ where $\xi = x, y, z$, we have:

$$\Psi_\xi(x,\boldsymbol{\rho}) = \exp\left[j\mathbf{K}\cdot x\hat{\mathbf{x}}\right] \sum_{\mathbf{G}\in G} \phi_\xi(x,\mathbf{G}) \exp\left[j(\mathbf{K}+\mathbf{G})\cdot\boldsymbol{\rho}\right] \tag{6}$$

being $\boldsymbol{\rho} = y\hat{\mathbf{y}} + z\hat{\mathbf{z}}$, $\hat{\mathbf{x}}$ is the unit vector along the x–axis, $\mathbf{K}$ is the complex wave vector characterized by a real part β which is the propagation constant of the wave and by an imaginary part α which takes into account the propagation losses due to Bragg reflection. The summation in Eq. (6) is performed over all the reciprocal lattice vectors $\mathbf{G}$ retained in the calculations. By substituting Eq. (6) into Maxwell's equations and taking into account the Eqs. (3,4), we obtain the following differential equation in matrix form:

$$\frac{d\mathbf{v_t}(x)}{dx} = \begin{bmatrix} \mathbf{O} & \mathbf{S_1} \\ \mathbf{S_2} & \mathbf{O} \end{bmatrix} \mathbf{v_t}(x) = \mathbf{M}\mathbf{v_t}(x) \tag{7}$$

where $\mathbf{v}_t(x)$ is the column vector whose elements are the tangential components of the electric and magnetic fields $\mathbf{E}_t$ and $\mathbf{H}_t$, respectively. As we will show next, in the final model equations only the matrix $\mathbf{S}_1$ is relevant and it's defined as:

$$\mathbf{S}_1 = \frac{1}{k_0}\begin{bmatrix} -\mathbf{K}_\mathbf{z}^\mathbf{G}\boldsymbol{\eta}\mathbf{K}_\mathbf{y}^\mathbf{G} & \mathbf{K}_\mathbf{z}^\mathbf{G}\boldsymbol{\eta}\mathbf{K}_\mathbf{z}^\mathbf{G} - k_0^2\mathbf{I} \\ k_0^2\mathbf{I} - \mathbf{K}_\mathbf{y}^\mathbf{G}\boldsymbol{\eta}\mathbf{K}_\mathbf{y}^\mathbf{G} & \mathbf{K}_\mathbf{y}^\mathbf{G}\boldsymbol{\eta}\mathbf{K}_\mathbf{z}^\mathbf{G} \end{bmatrix} \tag{8}$$

being k_0 the free space wavenumber, $\mathbf{I}$ is the diagonal identity matrix, $\mathbf{K}_\mathbf{z}^\mathbf{G}$ and $\mathbf{K}_\mathbf{y}^\mathbf{G}$ are diagonal matrices whose elements are all the vectors $\mathbf{K}^\mathbf{G} = \mathbf{K} + \mathbf{G}$ along the z and y directions, and $\boldsymbol{\eta}$ is the matrix with elements $\eta_{(n,m)} = \epsilon_G^{-1}(\mathbf{G}_n - \mathbf{G}_m)$, being $\mathbf{G}_n$ and $\mathbf{G}_m$ the n–th and m–th reciprocal lattice vectors, respectively. The solution of Eq. (7) takes the form of a matrix exponential:

$$\exp\left(\mathbf{M}\frac{t_g}{2}\right)\begin{bmatrix} \mathbf{E_t}(x_0) \\ \mathbf{H_t}(x_0) \end{bmatrix} = \exp\left(-\mathbf{M}\frac{t_g}{2}\right)\begin{bmatrix} \mathbf{E_t}(x_f) \\ \mathbf{H_t}(x_f) \end{bmatrix} \tag{9}$$

where x_0 and x_f are the coordinates of the bottom and top metal plate, respectively.

Since the matrix $\mathbf{M}$ assumes the special block–form given in Eq. (7), the matrix exponential can be represented in power series:

$$\exp\left(\pm\mathbf{M}\frac{t_g}{2}\right)=\sum_n\frac{t_g^{2n}}{(2n)!}\begin{bmatrix}\mathbf{P}_{12}^n & \pm\frac{t_g}{2n+1}\mathbf{P}_{12}^n\mathbf{S}_1\\ \pm\frac{t_g}{2n+1}\mathbf{P}_{21}^n\mathbf{S}_2 & \mathbf{P}_{21}^n\end{bmatrix} \tag{10}$$

where $\mathbf{P}_{ij}=\mathbf{S}_i\mathbf{S}_j$ is the matrix having size $2N_{\text{vect}}x2N_{\text{vect}}$, being N_{vect} the number of reciprocal vectors retained in calculations. By combining the previous Eqs. (9,10) and applying the boundary conditions on each ideal metal layer (i.e. $\mathbf{E}_t(x_0)=\mathbf{0}$, $\mathbf{E}_t(x_f)=\mathbf{0}$), we have:

$$\left[\sum_n\frac{t_g^{2n+1}}{(2n+1)!}\left(\sqrt{\frac{t_g^2}{4}\mathbf{P}_{12}}\right)^{2n}\right]\mathbf{S}_1\mathbf{H_t}\left(x_0\right)=\mathbf{0} \tag{11}$$

where $\mathbf{H}_t(x_0)=\mathbf{H}_t(x_f)$, as expected, being our structure symmetrical. As already stated, the $\mathbf{S}_2$ matrix does not contribute further to model equations.

Finally, the summation in Eq. (11) is the series expansion of the function $\sinh(z^{1/2})/(z^{1/2})$ applied to the complex matrix $(t_g/2)^2\mathbf{P}_{12}$ and since this function does never vanish, the only nontrivial solutions of Eq. (11) can be found by solving:

$$\det\left(\mathbf{S_1}\right)=0 \tag{12}$$

where $\mathbf{S}_1$ is a $2N_{\text{vect}}x2N_{\text{vect}}$ matrix. We can obtain a further numerical improvement by applying the following well known relationship holding for a $2x2$ structured block matrix:

$$\det\left(\begin{bmatrix}\mathbf{A} & \mathbf{B}\\ \mathbf{C} & \mathbf{D}\end{bmatrix}\right)=\det\left(\mathbf{A}\right)\cdot\det\left(\mathbf{D}-\mathbf{CA^{-1}B}\right) \tag{13}$$

where $\mathbf{A}$, $\mathbf{B}$, $\mathbf{C}$, $\mathbf{D}$ are matrices, and the term $\mathbf{D}-\mathbf{CA}^{-1}\mathbf{B}$ is the Schur complement of the block $\mathbf{A}$ [9]. By using the Eq. (13), the Eq. (12) becomes, after some calculations:

$$\det\left[\left(\left[\mathbf{K_z^G}\right]^2+\left[\mathbf{K_y^G}\right]^2\right)\boldsymbol{\eta}-k_0^2\mathbf{I}\right]=0 \tag{14}$$

which is a typical eigenvalue problem, easily solvable by using some efficient numerical methods. Moreover, the previous manipulation (13) halves the order of the matrices, thus improving the stability of the numerical approach which results fast and accurate also when a significant number of reciprocal vectors is retained in the calculations. After evaluating the edges of the irreducible Brillouin region, we have solved the Eq. (14) to investigate the photonic band diagram for the only TM–modes supported by the structure, as in the following section.

3 NUMERICAL RESULTS AND COMPARISONS

In order to obtain a given precision, we firstly need to evaluate the number of reciprocal grating vectors $\mathbf{G}$ to be retained in the calculations. In our numerical implementation the odd number N_{vect} of the retained reciprocal vectors is expressed as $N_{\text{vect}}=(2N_{\max}+1)^2$, being $N_{\max}$ a positive integer number. The numerical simulations, performed to calculate the first five bands of a 2D photonic crystal arranged as a square ($\gamma=\pi/2$) or hexagonal ($\gamma=\pi/3$) lattice having circular rods ($R=0.182a$, $\epsilon_a=9$) in air ($\epsilon_b=1$), reveal a relative error reduction of about 0.35% on the high order mode when the number of reciprocal vectors increases from $N_{\text{vect}}=625$ (i.e. $N_{\max}=12$) to $N_{\text{vect}}=729$ ($N_{\max}=13$). Therefore, if the bandgap is localized between low order modes, as in our cases, we do not require any further improvement in terms of precision and $N_{\text{vect}}=729$ reciprocal vectors is a good choice. We have implemented our model in GNU Octave high level language, running on a PC with 2.6 GHz Intel CPU and 1 GB RAM, platform based on a FEDORA–Red Hat 3 OS. The application of the Schur complement (13) allows to calculate the first five photonic bands on the irriducible Brillouin region in less then five minutes, also when a considerable discretization of the K axis (46 points) is used.

To validate our calculations, we have investigated the previous structure with the highly complex and accurate FDTD method [10], and compared the results with those obtained by using our numerical approach. As well known, the FDTD is rather difficult to be used to evaluate the band diagrams [11, 12] since it requires a very small discretization step both in time and frequecy domain. An important aspect is that the FDTD can fail at the symmetry points of the Brillouin zone, where some bands are degenerate and only one eigenvalue can be found.

Figure 2 shows the band diagram of the photonic crystal, based on a cubic lattice, computed by using our method (solid lines) and FDTD (crosses), and an excellent agreement is reached for each mode.

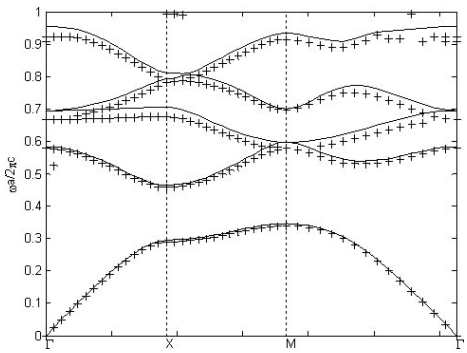

FIG. 2 Band diagram for a cubic lattice ($R=0.182a$, $\epsilon_a=9$, $\epsilon_b=1$) computed by using our method (solid) and FDTD (crosses).

In Table 1 we have reported the absolute and the percentage relative error for each of the five computed modes.

Band	E	e%
1 °	$\leq 10^{-2}$	2.6
2 °	0.02	3.4
3 °	0.03	4.1
4 °	0.03	4.1
5 °	0.04	4.1

TABLE 1 Absolute and percentage relative error for each of the five computed modes.

As discussed before, the large number of reciprocal grating vectors ($N_{\text{vect}} = 729$) provides a very small error in our numerical computation and the slight discrepance with FDTD results especially in the high order modes is due to the difficulty to optimize the input parameters required by the latter approach. We have also compared the two numerical methods in the investigation of a photonic crystal with hexagonal lattice arrangement, as shown in Figure 3, and a very good agreement can be observed also in this case. In this diagram several crosses are missing, and this aspect is due to the typical convergence problems of the FDTD near the symmetry points. The maximum relative error is lower than 4%, the discrepance relevant the third mode at the Γ point, where a degenerate point exists.

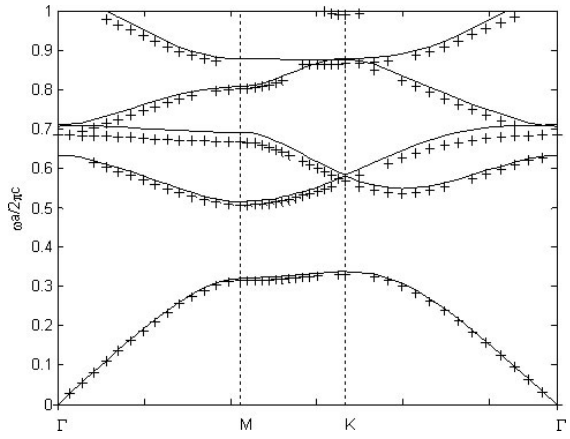

FIG. 3 Band diagram for a triangular lattice (R=0.182a, $\epsilon_a = 9$, $\epsilon_b = 1$) computed by using our method (solid) and FDTD (crosses)

After the accuracy of our formulation has been discussed, we now apply the approach to analyze some photonic structures characterized by a generic angle γ of inclination between the two primitive translation vectors. We derive easily the symmetry points of the irreducible Brillouin zone, as shown in Figure 4.

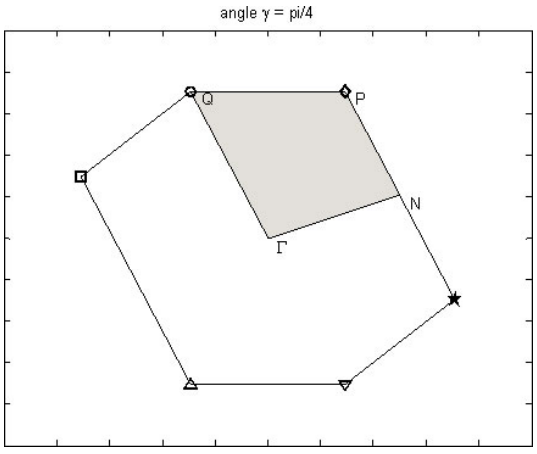

FIG. 4 Brillouin zone and irreducible Brillouin zone for generic inclination angle.

Because of the generic angle between the two primitive vectors, the Brillouin zone appears tilted and characterized by only two symmetry axes. This aspect provides a rather large irreducible region, characterized by four vertices, as shown in Figure 4.

The vertices of the irreducible Brillouin region can be easily calculated through the following relationships:

$$\begin{aligned}
\mathbf{\Gamma} &= \mathbf{O} \\
\mathbf{N} &= +\tfrac{\pi}{a}\hat{\mathbf{z}} - \tfrac{\pi}{a}\tfrac{1-\cos(\gamma)}{\sin(\gamma)}\hat{\mathbf{y}} \\
\mathbf{P} &= +\tfrac{\pi}{a}\tfrac{1}{1+\cos(\gamma)}\hat{\mathbf{z}} - \tfrac{\pi}{a}\tfrac{1}{\sin(\gamma)}\hat{\mathbf{y}} \\
\mathbf{Q} &= -\tfrac{\pi}{a}\tfrac{1}{1+\cos(\gamma)}\hat{\mathbf{z}} - \tfrac{\pi}{a}\tfrac{1}{\sin(\gamma)}\hat{\mathbf{y}}
\end{aligned} \tag{15}$$

The Brillouin zone becomes highly symmetrical for only two angles, $\gamma = \pi/3$ (hexagonal lattice) and $\gamma = \pi/2$ (square lattice): in these cases the irreducible Brillouin region can be further reduced giving a simple triangle, characterized by the canonical three symmetrical points Γ, M, K (triangular lattice) or Γ, M, X (square lattice).

The device designed is a PBG particle accelerator operating at about 15 GHz. The designed parameters values are: $a = 0.00858\ m$, $R = 0.00156\ m$, $t_g = 0.00460\ m$, $\epsilon_a = 9$, $\epsilon_b = 1$.

We have retained 225 harmonics in calculations, since a further increase of the harmonic number does not change significantly the results.

The first simulation is performed for an angle of inclination $\gamma = 45^o$, which corresponds to the Brillouin region depicted in Figure 4. The Photonic Band diagram, illustrated in Figure 5, shows a relatively large bandgap which extends from 13.4 GHz (i.e. $\omega a/2\pi c = 0.38$) to 17.4 GHz (i.e. $\omega a/2\pi c = 0.50$). The filling factor, defined by the Eq. (5), in this case is equal to 0.147 and provides a width of the first bandgap $\Delta G = 0.12$.

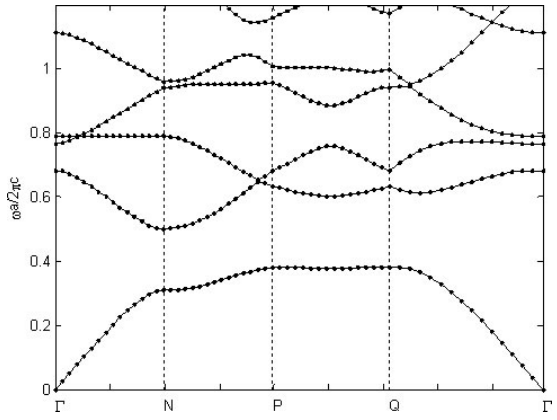

FIG. 5 Photonic band diagram for the only supported TM–modes of the structure characterized by a column permittivity e_a = 9 and filling factor $f = 0.147$.

We can improve the extension of the bandgap by choosing an optimal value of the filling factor, as sketched in Figure 6, which shows a maximum width of the bandgap occurring at a low value of the filling factor ($f = 0.147$). By changing the

angle γ of inclination we can obtain a further enlargement of the bandgap, as clearly shown in Figure 7, where the width of the forbidden frequency range has been plotted as a function of the filling factor for several values of γ.

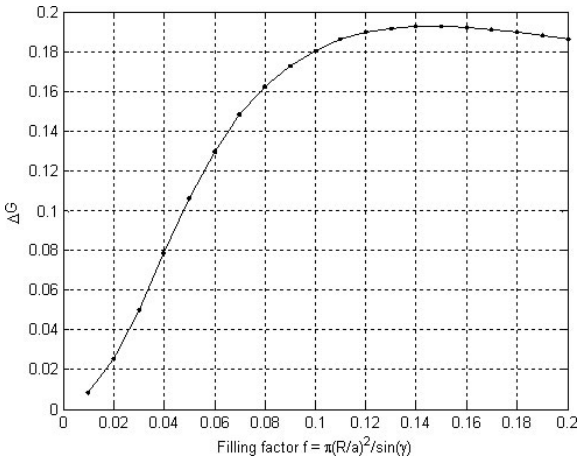

FIG. 6 The bandgap as a function of the filling factor.

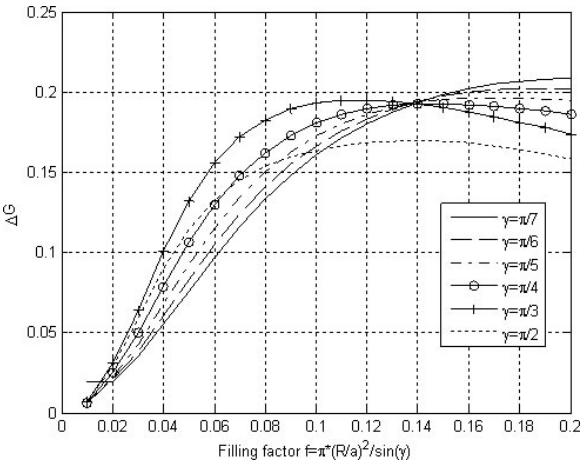

FIG. 7 Bandgap as a function of filling factor for several values of the angle of inclination γ.

As depicted in the diagram, the maximum value of the bandgap width strongly depends on the inclination angle, and this behavior is confirmed by the Figure 8 where the optimal bandgap extension has been represented as a function of γ. Figure 8 also shows a repetition of the curve starting from the angle $\gamma = \pi/3$ and a good choice for the angle should be $\gamma \leq 0.6$.

Figure 9, which is related to a periodic structure characterized by an angle of inclination $\gamma = 0.4$ radians, shows the bandgap width as a function of the filling factor for several values of rod dielectric constant ϵ_a. The increase of the rod permittivity ϵ_a produces an enlargement of the bandgap but does not change remarkably the value of filling factor in which the maximum occurs.

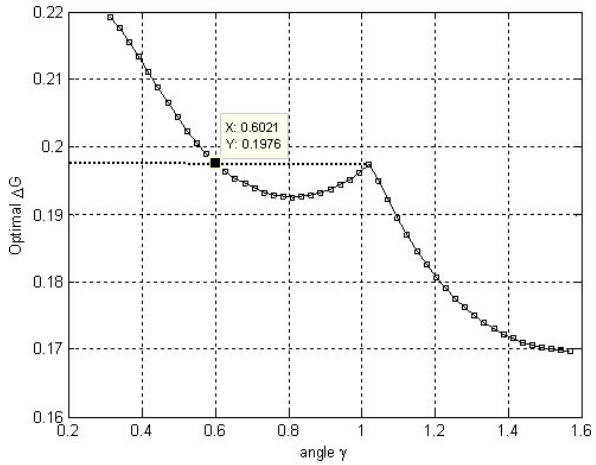

FIG. 8 The bandgap as a function of the angle of inclination γ at the optimum value of the filling factor.

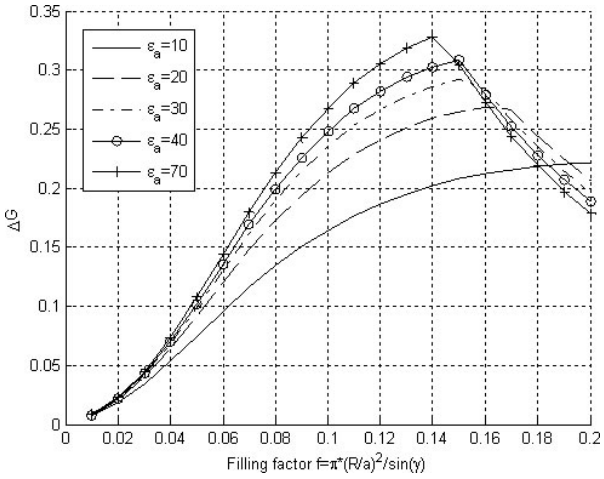

FIG. 9 Bandgap as a function of the filling factor for several values of cylinders dielectric constant ϵ_a.

For a large value of rod dielectric constant ($\epsilon_a = 20$) we have chosen the optimal value of filling factor ($f = 0.15$) from the Figure 10, and applied it to perform the calculations of the Photonic Band diagram illustrated in Figure 11.

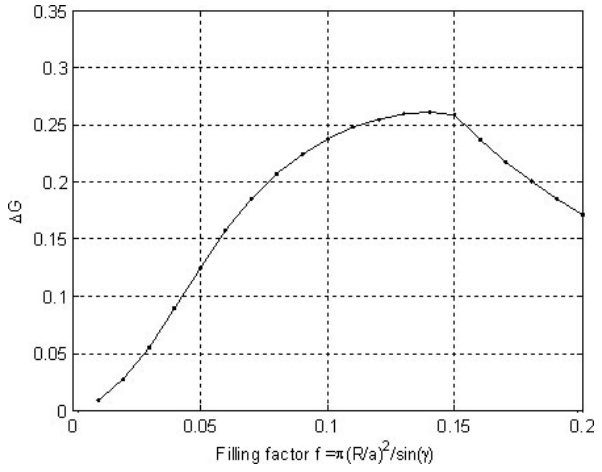

FIG. 10 Bandgap as function of the filling factor for $\gamma = 0.4$.

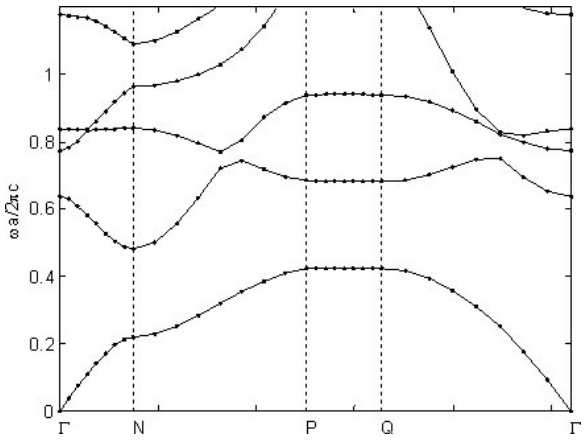

FIG. 11 Photonic Band diagram for a periodic structure with $\gamma = 0.4$ and rod permittivity $\epsilon_a = 20$

4 CONCLUSIONS

We have presented a numerical method, based on the well known Floquet–Bloch theory, useful to analyze the physical properties of a PBG based accelerator, working at microwave frequency range. So far, models based on the Floquet–Bloch theory and oriented to analyze PBG structures have been applied only to highly symmetrical lattices, characterized by hexagonal or square unit cells and in the literature different typologies are not considered. Our model, on the contrary, takes into account a large number of geometrical parameters and, in particular, the inclination of the unit cell which can assume any value in the range 0–90 degrees.

The model and its numerical implementation is characterized by the absence of any a priori assumptions, thus allowing a fast ad accurate determination of several informations on the design parameters required to optimize the device performances.

We have compared our method with the well known and accurate FDTD, which is not suitable for analyzing structures with generic inclination angle, since the boundary conditions on the method require a rectangular numerical domain in which the computation has to be processed. As well known, a lattice characterized by a generic unit cell cannot always be reduced to a square or rectangular domain. This aspect limits the use of the FDTD with respect to our method.

The comparisons show a small shift of about 4% on the high order modes, we have applied the method to investigate the influence on the photonic band structure of the angle between the two primitive translation vectors, the filling factor and the rod permittivity. Best results in terms of bandgap width can be obtained by choosing an inclination angle smaller than $\gamma = 0.6$, a value significantly smaller than that of the conventional lattice with hexagonal symmetry.

References

[1] E. I. Smirnova, C. Chen, M. A. Shapiro, R. J. Temkin, "An 11 GHz Photonic Band Gap accelerator structure with wakefield suppression" Proceedings of the 2003 Particle Accelerator Conference, 1258–1260.

[2] M. A. Shapiro, E. I. Smirnova, C. Chen, R. J. Temkin., "Theoretical analysis of overmoded dielectric photonic band gap structures for accelerator applications" Proceedings of the 2003 Particle Accelerator Conference, 1255–1257.

[3] A. Giorgio, A. G. Perri, M. N. Armenise, "Very fast and accurate modelling of multilayer waveguiding photonic band-gap structures" J. Lightwave Technol. **19**, 1598–1613 (2001).

[4] A. Giorgio, D. Pasqua, A. G. Perri, "Multiple Defect Characterization in Finite-Size waveguiding Photonic Band-Gap Structure" IEEE J. Quantum Elect. 1537–1547 (2003).

[5] V. M. N. Passaro, R. Diana, M.N. Armenise, "Optical fiber Bragg gratings. Part I. Modeling of infinitely long gratings", J. Opt. Soc. Am. A, Vol. **19**, 1844–1854 (2002).

[6] V. M. N. Passaro, R. Diana, M. N. Armenise, "Optical Fiber Bragg Gratings. Part II: Modeling of Finite Length Gratings and Grating Arrays" J. Opt. Soc. Am. A, Vol. **19**, 1855–1866 (2002).

[7] R. Diana, A. Giorgio and A. G. Perri, "Theoretical Characterization of Multilayer Photonic Crystals having a 2D periodicity" Int. J. Numer. Model. El. 365–382 (2005).

[8] J. D. Joannopoulos, R. D. Meade, J. N. Winn, *Photonic Crystals* (Princeton University Press 1995).

[9] D. Serre, *Matrices: Theory and Applications* (Springer-Verlag, New York 2002).

[10] A. Taflove, *Computational Electrodynamics: The Finite-Difference Time-Domain Method* (Norwood, MA: Artech House 1995).

[11] M. Boroditsky, R. Coccioli, and E. Yablonovitch, "Analysis of photonic crystals for light emitting diodes using the finite differences time domain technique" in Proc. SPIE **3283**, 184–190 (1998).

[12] A. J. Ward and J. B. Pendry, "A program for calculating photonic band structures, Green's functions and transmission/reflection coefficients using a nonorthogonal FDTD method" Comp. Phys. Commun. **128**, 590–621 (2000).